Formulation induces direct DNA UVA photooxidation. Part I. Role of the formulating cationic surfactant

Johanne Teychené, Dalina Didacus-Prins, Nadia Chouini-Lalanne, Valérie Sartor, Christophe Dejugnat

Formulation induces direct DNA UVA photooxidation. Part I. Role of the formulating cationic surfactant

Johanne Teychené, Dalina Didacus-Prins, Nadia Chouini-Lalanne, Valérie Sartor, Christophe Déjugnat**

Laboratoire des IMRCP, Université de Toulouse, CNRS UMR 5623, Université Toulouse III - Paul Sabatier

Abstract

Cethyltriethylammonium bromide (CTEAB) was considered as a cationic surfactant to form lipoplexes with DNA. In TRIS/HCl buffer, CTEAB self-assembles above its critical micelle concentration (CMC = 0.15 mM) into small spherical micelles as determined by complementary scattering techniques. This surfactant readily interacts with the supercoiled plasmid DNA pBR322 *via* electrostatics and hydrophobic interactions. Upon increasing surfactant concentration, successive phase transitions are observed from partial neutralization to full compaction of DNA as evidenced by agarose gel electrophoresis, tensiometry, pyrene fluorescence, UV-Vis absorbance and circular dichroism measurements. Under UVA radiation (λ ≥ 335 nm), we show that the presence of the surfactant increases photooxidized damage on DNA

especially in the compacted state. A mechanistic study using selective scavengers shows the involvement of singlet oxygen in these oxidative processes due to the direct UVA absorption of DNA itself.

Keywords

surfactant; self-assembly; DNA; formulation; UVA photosensitization

*corresponding author: Dr. Christophe Déjugnat, dejugnat@chimie.ups-tlse.fr

1. Introduction

If gene therapy opens up new therapeutic perspectives in the treatment of inherited deficiency diseases (*e. g.* cystic fibrosis), acquired diseases (cancer, neurodegenerative diseases) or infectious diseases (hepatitis, AIDS), its success depends on the effective transmission and expression of genetic material within cells. This undoubtedly requires the development of systems capable of efficiently and safely crossing biological barriers on the way to the nucleus and transmitting the drug gene there. Most of the systems used involve recombinant viral vectors, capable of inserting efficiently the transgene into the cells. Although the latter are very effective in the transfer function, their use has a number of disadvantages (production cost, safety, development of immune reactions, and risk of pathogenicity). To avoid them, a number of synthetic vectors have been developed. They are mostly cationic derivatives of a lipidic or polymeric nature capable of interacting with DNA by electrostatic interactions and compacting it to form particles (aggregates).[1] Moreover, since the effective charge of the DNA and its size are reduced, the efficiency of the transfer of the drug gene to its site of action is also improved.

In the case of the *in vivo* delivery, the compacted gene/vector system can be transferred to the target DNA in two ways: either by the systemic route or by local application.[2] However, whatever the mode of administration, the gene must be associated with a system capable of protecting it against aggression by the external environment and in particular from UV radiation, one of the main sources of DNA damage at the origin of photocarcinogenesis processes. While the photomutagenic potential of UVB radiation has long been established, that of UVA radiation, which is longer and deeper penetrating the skin, has only recently been recognized. Indeed, the direct formation of cyclobutane pyrimidine dimers (CPD) in DNA under UVA

radiation has been widely reported[3–12] and the involvement of UVA radiation in cancer and skin aging processes is now well established. However, no study has been carried out on the direct influence of UVA radiation on DNA in a synthetic vector system. Yet DNA delivery in the skin could be affected by sunlight. The studies carried out in this sense involved the presence of a photosensitizer and focused on studying the influence of the formulation on the formation of photoinduced oxidized damage[13] while the direct absorption of UVA radiation by DNA has been widely demonstrated. So, the purpose of this work is to focus on the direct formation of oxidized lesions on DNA formulations under UVA radiation involving as cationic derivatives, a close analog of cetyltrimethylammonium bromide (CTAB), namely cetyltriethylammonium bromide (CTEAB, Figure 1).

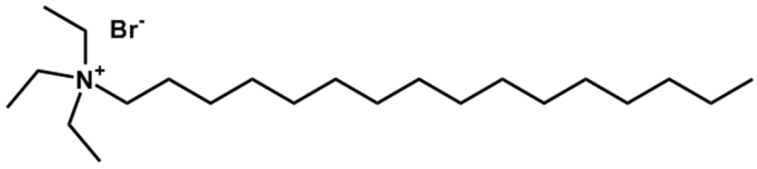

Figure 1. Structure of cetyltriethylammonium bromide (CTEAB).

This cationic surfactant presents the advantage of being readily soluble in liquid water at any temperature (T_{Krafft} < 0 °C),[14] whereas the Krafft temperature of CTAB (T_{Krafft} = 25 °C)[14] could be the source of troubles when handling it at room temperature (close to the solubility temperature). On the other hand, CTEAB presents a bulkier head group than CTAB and this affects its self-organization properties in pure water due to molecular packing considerations.[15] For example, although they have similar critical micelle concentrations (CMCs) in water, CTAB

77 forms elongated micelles while CTEAB rather self-assembles into much smaller,
78 slightly ellipsoidal micelles.[16,17] Therefore CTEAB has been mainly used as pore
79 directing agent for the preparation of mesoporous materials thanks to its ability to
80 form micellar cubic phases,[18–20] but also as adjuvant in enhancing oil recovery
81 technique.[21,22] However its interaction with DNA has not been reported yet (few
82 authors sometimes describe the use of cetyltriethylammonium bromide in DNA
83 extraction and purification processes, but a closer look shows that it was a
84 misspelling of cetyltrimethylammonium bromide, which is widely used for decades in
85 reference protocols). Therefore, it is interesting to consider this CTEAB-DNA
86 formulation and to see whether the slight structural change (ethyl *vs* methyl) due to
87 the replacement of CTAB by CTEAB could induce significant changes or not.
88 In a first part we present the self-organization properties of CTEAB in the buffer
89 solution used as solvent for DNA. Indeed, aggregation of CTEAB has been depicted
90 in water but the presence of electrolytes (buffer) is known to have an impact on such
91 properties.[23] Therefore the determination of the CMC (by tensiometry and pyrene
92 fluorimetry) and the depiction of the micelles (by scattering experiments) will be
93 carried out. Then the CTEAB-DNA interactions will be characterized to check that
94 CTEAB can also be used to formulate DNA, as an analog of CTAB. For that, the
95 critical aggregation concentrations (CACs) will be determined by complementary
96 techniques (tensiometry, pyrene fluorimetry, agarose gel electrophoresis, UV-Vis
97 absorbance and circular dichroism measurements). Finally, we will investigate the
98 effects of UVA radiation on these formulations (by agarose gel electrophoresis) and
99 will evidence that it can led to direct DNA photosensitization. Experiments conducted
100 in the presence of peculiar scavengers will allow a mechanistic interpretation of the
101 results obtained.

2. Materials and methods

2.1. Materials

Triethylamine (purity 99.9 %) and 1-bromohexadecane (purity 98%) were purchased from VWR (Fontenay Sous Bois, France) and Lancaster (Morecambe, England), respectively. CTEAB was synthesized as described in the literature[24] and purification protocol was improved. Briefly, 1-bromohexadecane (20 g, 65 mmol) was reacted with triethylamine (10 mL, 72 mmol) in 130 mL absolute ethanol for 72 h at 85 °C (reflux). After evaporation to dryness under reduced pressure, the residue was dissolved in chloroform and ethyl acetate was added to induce precipitation. After precipitation was completed at 4 °C, the white solid was collected by filtration and washed with ethyl acetate. Final purification was achieved by solid phase extraction (SPE) on a reverse phase Chromabond C_{18} ec chromatographic column (70 mL, 10 g) from Macherey-Nagel (first washing with water then elution with methanol). This step ensured full removal of the impurity trimethylamine hydrobromide. Evaporation of methanol afforded CTEAB as a white crystalline solid. Purity was assessed by nuclear magnetic resonance (NMR) and high-resolution mass spectroscopy (HRMS). (see *Supporting Information*).

Tris(hydroxymethyl)aminomethane (TRIS, purity 99.8 %) was from Fisher Scientific (Geel, Belgium). Supercoiled plasmid DNA (Form I) pBR322 (4361 base pairs) was purchased from Thermo Fisher Scientific (Vilnius, Lithuania), stored in 10 $\times 10^{-3}$ mol.L^{-1} of TRIS/HCL (pH 7.6) and 1×10^{-3} mol.L^{-1} of EDTA. The DNA was used after dilution in a 20 mM TRIS/HCl buffer (pH=7.4) to obtain a stock solution at [DNA-PO_4^-] = 4.5×10^{-4} mol·L^{-1}. All the DNA concentration indicated on the manuscript are in mol phosphate·L^{-1}. Heparin sodium salt (purity 99.8%) was purchased from Alfa Aesar (Heysham, Germany) and Sodium azide (NaN_3, purity 99%) from Alfa Aesar

(Karlsruhe, Germany). Agarose and tert-butanol (^{t}BuOH, purity 99.5%) were obtained from Sigma-Aldrich (Saint Louis, USA), while pyrene (purity 98%) was from Acros Organics (Geel, Belgium). Ethidium Bromide (EB) was purchased as a 10 mg·mL^{-1} aqueous solution from Invitrogen (Carlsbad, USA). D_2O (purity 99.9%) was obtained from Eurisotop (Saint Aubin, France) and T4 endonuclease V (pyrimidine dimer glycosylase) from BioLabs (New England, USA). Bromophenol blue was purchased from Sigma Aldrich (Saint Louis, USA).

Water used in all experiments was produced by a two-stage Milli-Q filtration system from Millipore and had a resistivity higher than 18.2 MΩ·cm.

2.2. Surface tension measurements

Surface tension measurements were performed using a Krüss EasyDyne tensiometer using the Wilhelmy plate method. Temperatures were maintained at 25 °C (± 0.1 °C) by circulating thermostated water through a jacketed vessel containing the solution. For each experiment, surface tension was measured three times (each time ten readings were performed and averaged) after an equilibration time of 30 minutes.

2.3. Fluorescence measurements

A stock solution of pyrene (10^{-4} mol·L^{-1}), was prepared in methanol and stored in glass vials at 4 °C. The solutions for fluorescence probing studies were prepared by adding 1 µL of this pyrene stock solution (10^{-4} mol·L^{-1}) to 399 µL of the sample solution. Final concentration of pyrene was 2.5×10^{-7} mol·L^{-1}, while the amount of methanol remained very low (0.25 % vol.) Fluorescence measurements were performed on a Fluorolog Horiba spectrofluorimeter equipped with channel multiple tau correlator (auto and cross correlation, 1088 real time channels) and a

thermostated cuvette holder at 25 ± 0.1 °C. Excitation wavelength was 335 nm, and the fluorescence emission was recorded between 350 and 500 nm.

2.4. UV-Visible absorbance and circular dichroism measurements

Absorption spectra were recorded on a Hewlett Packard HP 8452A Diode Array Spectrophotometer with an optical path length of 1 cm.

Circular dichroism spectra were obtained from a circular dichroism spectrometer J-815 from Jasco equipped with a 150 W Xenon arc lamp light source, using a bandwidth of 0.5 nm, with medium sensitivity with a maximum of 200 mdeg. Data acquisition was done in continuous mode.

2.5. Multi-angle light scattering experiments

The multi-angle light scattering (MALS) measurements were performed on a 3D LS Spectrometer from LS Instruments (Fribourg, Switzerland) equipped with a 100 mW high performance DPSS Laser (Cobolt) operating at λ = 660 nm, a two-channel multiple tau correlator (auto and cross correlation, 1088 real time channels), a 3D cross-correlation module, a variable-angle detection system, two high sensitivity APD detectors, an automated laser attenuation system combined with on-line laser intensity measurement, a temperature controllable sample chamber with index matching vat, and an external circulator for temperature control (Julabo CF31).

Before analysis (and otherwise stated), samples were filtered through 0.2 µm hydrophilic PTFE filters into the cylindrical scattering cells.

Measurements were performed at 25°C for scattering angles θ ranging from 12° to 150°, corresponding to scattering wave vectors q in the range from 2.7×10^{-3} to 2.4×10^{-2} nm^{-1}. As CTEAB solutions did not produce multiple scattering, the 3D-cross

correlation configuration was not required and the measurement were performed in the classical 2D-pseudo cross configuration.

At each angle, 3 to 10 measurements were carried out and later averaged after having discarded eventual meaningless correlograms. Analysis of both dynamic and static light scattering measurements were performed using the home-made MULTI-STORMS software developed by Dr. C. Mingotaud (see *Supporting Information*).

2.6. Small-Angle X-ray Scattering experiments

SAXS (Small-Angle X-ray Scattering measurements) were conducted at the European Synchrotron Radiation Facility (ESRF, Grenoble, France) at the ID02 beamline. CTEAB solutions (5 to 20 mM) were transferred into glass capillaries before measurements. The sample-to-detector distance was 2.5 m. Using 1 Å X-ray wavelength, the q range covered was 2.9×10^{-3} Å^{-1} < q < 3.1×10^{-1} Å^{-1}. For each solution, 10 scans were recorded and averaged. For each scan, exposure time was kept as low as 100 ms to prevent from radiation damage. The observed intensities *I(q)* were corrected for transmission, solvent, and detector response. The analysis of the *I(q)* profiles was performed using the SasView software (http://www.sasview.org/).

2.7. Irradiation experiments

DNA irradiation was made with a Mercury Xenon lamp (Oriel instruments, 500W) equipped with a long pass filter λ ≥ 335nm (Newport 20CGA-335 GC505) at 20°C.

The irradiated and non-irradiated sample volume was 100 µL. The final concentrations in TRIS/HCl buffer (20 mM, pH=7.4) were 9×10^{-5} mol phosphate·L^{-1} for the plasmid DNA pBR322, from 0 to 4×10^{-3} mol·L^{-1} for the CTEAB solutions,

196 200×10^{-3} mol L^{-1} for NaN_3 and 4% v/v for ^{t}BuOH. Each experiment was at least
197 triplicated.
198
199 **2.8. Agarose gel electrophoresis**
200 2.8.1. Sample preparation
201 50 µL of the sample solution were used on the T4 endonuclease V experiment. It
202 consists to add 10 µL of T4 endonuclease V (10000U/ml) and to incubate the solution
203 30 minutes at 37°C. 5 µL of bromophenol blue solution and 10 µL of Heparin 20%
204 (w/w in TRIS/ HCl buffer (20 mM, pH= 7.4) were added.
205 To the samples without T4 endonuclease V treatment, 5 µL of bromophenol blue
206 solution, 10 µL of Heparin 20% (w/w in TRIS/ HCl buffer) and 10 µL TRIS/ HCl buffer
207 (20 mM, pH= 7.4) were added.
208 2.8.2 Electrophoresis and photodensitometry
209 An aliquot of 40 µL of each sample was deposited into 0.8% agarose gel containing
210 0.02 % of Ethidium Bromide. Electrophoresis migration was carried out for 4 hours
211 under a constant electric field of 80 mV.
212 Single strand breaks (SSB) were quantified by photodensitometry using the ImageJ
213 software. To correct the lower efficiency of ethidium bromide binding to Form I DNA
214 with respect to Form II, a coefficient of 1.66 was used.[25]
215

3. Results and discussion

3.1. Self-organization of CTEAB in TRIS/HCl buffer

CTEAB surfactant (Figure 1) was synthesized as described in the literature[24] and dissolved in 20 mM TRIS/HCl buffer solutions at pH = 7.4. Determination of the CMC by tensiometry was performed by measuring the variation of the surface tension as a function of the surfactant concentration. In the dilute regime, the surface tension value is close to the one of water and then it decreases when the concentration of surfactant increases. At the threshold value which corresponds to the CMC, the surface tension does not vary much upon increasing surfactant concentration (Figure 2A).

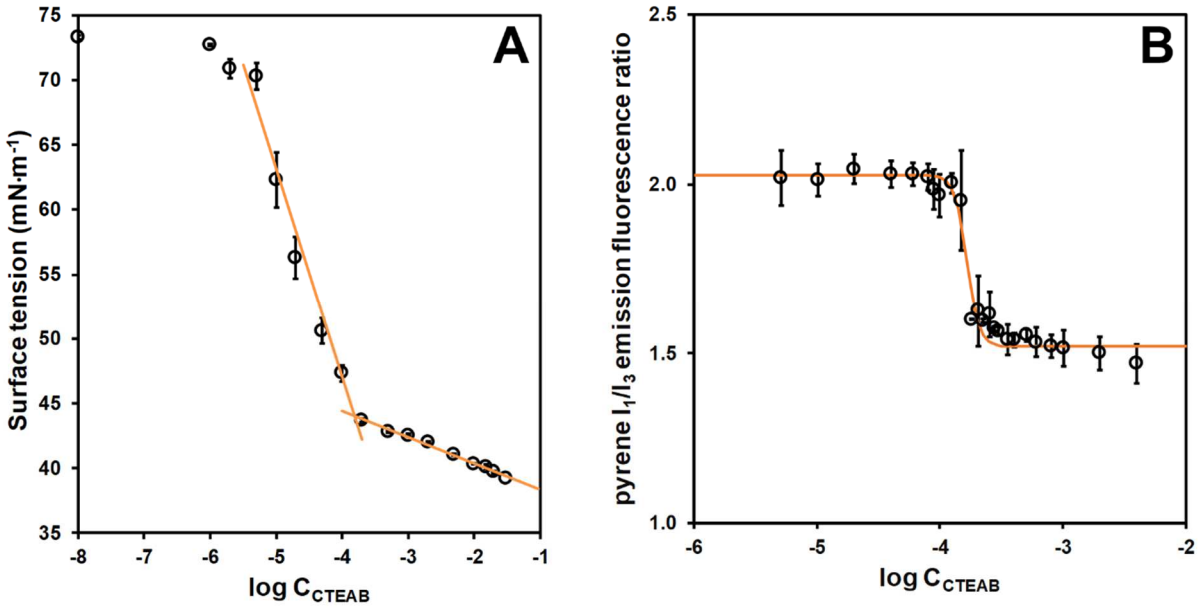

Figure 2. Variation of the surface tension (A) and of the pyrene I_1/I_3 fluorescence emission ratio (B) of CTEAB solutions as a function of the CTEAB concentration in 20 mM TRIS/HCl buffer (pH = 7.4) at 25 °C.

By this technique the CMC of CTEAB was found to be 1.5 (± 0.2) $\times 10^{-4}$ mol·L^{-1} in the 20 mM TRIS/HCl buffer (pH = 7.4) at 25 °C. This value is much lower than the CMC

values reported in the literature for CTEAB in water: 7-8×10^{-4} mol·L^{-1}, as determined from tensiometry and conductivity experiments.[16,17,26–29] This decrease of CMC means that the aggregation is favored in TRIS/HCl buffer compared to pure water. The effect of the electrolyte is to partially screen the repulsion electrostatic interactions between the similar charged head groups of the surfactant and therefore to promote aggregation. Thereby, the CMC is lowering by addition of electrolyte.

In the same way, Haq, Z. and coworkers [30] reported a decrease of the CMC of the CTAB from 0.98 mol·L^{-1} (at 303 K) to 0.90 mol·L^{-1} at 3 mol·L^{-1} of NaCl, indicating the significant role of the electrostatic interactions between surfactant and electrolyte.

From the tensiometry curve, one can also estimate the minimal molecular cross-sectional area at the air/water interface $A_{s,min}$ at the CMC.[23] This is done using the Gibbs equation which relies the maximal surface excess concentration Γ_{max} to the slope of the surface tension *vs* log C curve before the CMC as follows:

$$\Gamma_{max} = -\frac{1}{2.303nRT} \cdot \frac{\partial \gamma}{\partial logC} \quad (1)$$

where T is the temperature, R the gas constant, C the concentration, and n the number of adsorbed species (here n = 2, accounting for $CTEA^+$ and Br^-). Then $A_{s,min}$ can be expressed as (2):

$$A_{s,min} = \frac{1}{N_A \Gamma_{max}} \quad (2)$$

where N_A is the Avogadro number. Applying this to the curve in Figure 2A gives $A_{s,min}$ = 110 (± 10) $Å^2$·$molecule^{-1}$. This value is quite high compared to a surface of 62 $Å^2$·$molecule^{-1}$ reported for CTEAB in pure water,[29] suggesting that the distance between the surfactants got increased at the interface in the presence of electrolytes. The fact that the interface occupation appears less compact (and the surfactants

bulkier) might be due to the accumulation of species (like water or ions) between the surfactants.

The aggregation properties of CTEAB in TRIS/HCl buffer have also been studied by pyrene fluorescence measurements. Pyrene is a hydrophobic fluorescent probe that has been widely used for the characterization of self-assembling systems due to the specific variation of its emission fluorescence as a function of the local polarity.[31] In its specific multi-peak emission spectrum, the I_1/I_3 intensity ratio between the first and third peaks (I_1 at 372 nm and I_3 at 383 nm respectively) is decreasing if the polarity decreases. In surfactant systems, this I_1/I_3 ratio varies as a function of the surfactant concentration with a sharp decrease at the CMC, from a high value (below CMC, pyrene located in water) to a lower one (above CMC, pyrene located in the hydrophobic inner core of the micelles). The results regarding pyrene fluorescence as a function of CTEAB concentration in TRIS/HCl buffer are represented in Figure 2B. The variation of the I_1/I_3 ratio has been adjusted by a sigmoidal Boltzmann function to determinate the CMC.[32]

From this fluorescence measurements, the aggregation of CTEAB in TRIS/HCl buffer occurs at CMC = 1.6 (± 0.2) $\times 10^{-4}$ mol·L^{-1}, which is in good accordance with tensiometry measurements (using this quick technique we also checked the CMC of CTEAB in pure water and found 7.1 (± 0.2) $\times 10^{-4}$ mol·L^{-1}, which is very close to the values reported in the literature,[16,17,26–29] see *Supporting Information, Figure S3*). In addition, the intrinsic value of the I_1/I_3 ratio is directly related to local micropolarity: a low ratio value (<1) indicates that pyrene is surrounded by a nonpolar environment, while higher ratio values (>1) show that the pyrene environment is polar.[31] This ratio has been shown to vary from about 0.6 in alkanes to 1.2-1.6 in alcohols and up to 1.9 in water.[31,33] In the present case of CTEAB, we observed a decrease of the I_1/I_3 ratio

279 from 2.0 to 1.5 at the CMC. This shows that even when located in micelles, the
280 pyrene probe is still in a rather polar environment. This suggest that water molecules
281 have partially penetrated the inner micellar cores, leading to an increase of the I_1/I_3
282 ratio. [31,34] This is directly related to the surfactants head groups: bulky heads induce
283 less compact interfaces and allow penetration of water, which is here consistent with
284 large polar surface areas determined for CTEAB from tensiometry measurements.
285 In order to get more insights on the structure of the aggregates formed by
286 CTEAB in aqueous TRIS/HCl solutions, both multi-angle static- and dynamic light
287 scattering (MASLS and MADLS) experiments were performed at different
288 concentrations ([CTEAB] = 5 to 30×10^{-3} mol·L^{-1}). Small angle X-Ray scattering
289 (SAXS) measurements were also carried out.
290 In light scattering experiments, the scattering wave vector q is defined as a function
291 of the scattering angle θ as described by equation (3).

$$q = \frac{4\pi n \sin(\theta/2)}{\lambda} \quad (3)$$

292 where n is the refractive index of the medium and λ the wavelength of the incident
293 light.
294 In MASLS, the excess of scattered intensity by a sample with respect to the
295 solvent is converted into absolute intensity (Rayleigh ratio R_θ, in cm^{-1}) using toluene
296 as a reference (see *Supporting Information*). Absolute Rayleigh excess ratios of
297 CTEAB solutions were measured in the 2.6×10^{-4}-2.5×10^{-3} Å^{-1} q range. In all cases,
298 flat plateaus were obtained meaning that the scattering was isotropic and that the
299 aggregates formed by CTEAB were very small in size (see *Supporting Information,*
300 *Figure S4*). As a consequence, the radius of gyration R_g could not be determined due
301 to the q-independent form factor in this q range. However, the variation of the
302 Rayleigh ratio as a function of the CTEAB concentration could allow Debye analysis

(see *Supporting Information, Figure S5*). Therefore, the apparent mass of the aggregates was determined to be M_w = 41.1 ± 1.6 kDa. From this value and using the molar weight of CTEAB, it was possible to calculate the aggregation number (N_{agg}) which was found to be N_{agg} = 101 ± 4. This value is larger or equal to those reported for CTEAB in pure water (N_{agg} = 49-100),[17,29] confirming that micellization in TRIS buffer is favored and allows a larger number of surfactant molecules to aggregate.

What is measured experimentally in MADLS is the autocorrelation function $g^{(2)}(q,\tau)$ of the scattered intensity $I(q,t)$, normalized over time (4):

$$g^{(2)}(q,\tau) = \frac{\langle I(q,t)I(q,t+\tau)\rangle}{\langle I(q,t)\rangle^2} \quad (4)$$

This latter is also related to the correlation function of the electric field $g^{(1)}(q,\tau)$ by the Siegert relationship (5):

$$g^{(2)}(q,\tau) = 1 + \beta\left|g^{(1)}(q,\tau)\right|^2 \qquad \beta \leq 1 \quad (5)$$

For monodisperse spherical particles under Brownian motion, the autocorrelation function decays exponentially over time (6):

$$g^{(1)}(q,\tau) = \mathrm{e}^{-\Gamma\tau} \quad (6)$$

where $\Gamma = D_0 q^2$ is the decay rate and D_0 is the translational diffusion coefficient of the particles. The hydrodynamic radius of equivalent sphere (R_h) is then obtained by the Stokes-Einstein relationship:

$$R_h = \frac{kT}{6\pi\eta D_0} \quad (7)$$

where k is the Boltzmann constant, T the absolute temperature, and η the solvent viscosity.

Experimentally, simple scattering was always observed (no multiple scattering) from the clear, transparent CTEAB solutions. In all cases, the autocorrelation functions were well fitted using a Cumulant analysis[35] (see *Supporting Information, Figure S6*),

affording the intensity-weighted decay rates Γ. Plotting decay rates as a function of q^2 afforded linear profiles $\Gamma = D_{app}q^2$ (Figure 3A), meaning that single relaxation mechanisms were observed associated to single apparent translational diffusion coefficients (D_{app}).

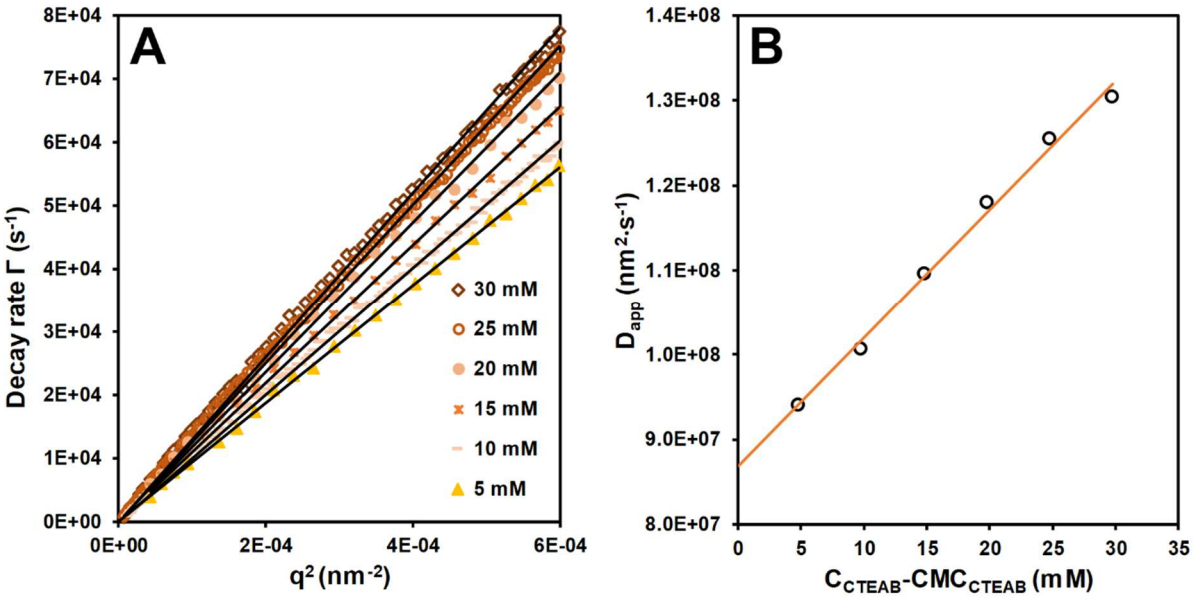

Figure 3. Linear variations of decay rates as a function of q^2 (A). Variation of the apparent diffusion coefficient D_{app} as a function of the micelle concentration (B).

The apparent diffusion coefficients showed a linear dependence as a function of the micelle concentration (*ie* C_{CTEAB}-CMC_{CTEAB}) (Figure 3B):

$$D_{app} = D_0 + k(C_{CTEAB} - CMC_{CTEAB}) \quad (8)$$

This reflects inter-particle interactions (probably electrostatic repulsions between positively charged aggregates of cationic surfactants). Extrapolation at infinite dilution afforded D_0= 8.68×10^7 nm^2·s^{-1} and $R_{h,0}$ = 2.83 nm from the Stokes-Einstein

relationship. This hydrodynamic radius is comparable to the dimensions of micelles formed by CTEAB in pure water.[16,17]

Knowing the radius of the micelles, the determination of their surface gives 101 nm^2, and dividing it by the aggregation number, the surface occupied by one surfactant head group is 1 nm^2, which is consistent with the surface estimated from tensiometry measurements. It was also possible to determine the volume occupied per surfactant at 0.94 nm^3. The comparison of this value to the molecular volume of CTEAB (0.64 nm^3) indicates that about 10 water molecules are present around each CTEAB molecule, confirming that CTEAB micelles are highly hydrated.

Complementary SAXS experiments were also carried out to get more information on CTEAB micelles. The general expression of the scattered intensity $I(q)$ is:

$$I(q) = \Phi \cdot \mathrm{V} \cdot (\Delta\rho)^2 \cdot P(q) \cdot S(q) \quad (9)$$

where $q = [4\pi \sin(\theta/2)]/\lambda$ is the scattering vector (θ is the scattering angle), Φ is the volume fraction of the scatterers, V is their volume, and $\Delta\rho$ is their difference in scattering length density (SLD) with respect to the solvent. $P(q)$ is the scatterers' form factor for which analytical expressions have been reported for various geometries.[36,37] $S(q)$ is the structure factor accounting for inter-particle interactions, for which different models are also available.[36,37] Regarding the CTEAB solutions, the scattering intensities were very low, indicating a weak electronic contrast between the solvent and the aggregates. Moreover, the profiles of the scattering curves suggested a spherical shape for the aggregates, as illustrated in Figure 4 (full curves and fitting parameters are reported in the *Supporting Information*).

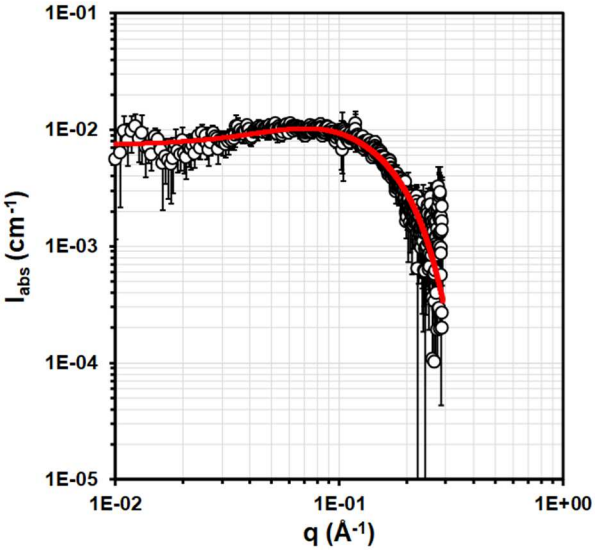

Figure 4. SAXS profile of 20 mM CTEAB solution in 20 mM TRIS/HCl (pH = 7.4) at 25 °C. The solid line represents the adjustment of the data with a spherical form factor and a structure factor of a charged hard sphere.

Indeed, the data were efficiently adjusted using a P(q) spherical model, whereas the ellipsoidal model used by others to describe CTEAB micelles in pure water was not convenient here.[16,17] In addition, a structure factor S(q) was included, which corresponded to a charged hard sphere model to take into account electrostatic repulsions between positively charged micelles (visible at low q as a decline of $I(q)$ in the SAXS curve). However, the classical core-shell structure could not be evidenced contrary to analogous cationic surfactants.[38] Instead, the SAXS profiles rather corresponded to small spherical shapes (R = 14 Å) with a scattering contrast that was the one of pure hydrophobic alkyl chains. This indicates that only a part of the inner core of the micelles could be observed by this technique, and it is again in accordance with a possible penetration of water towards the inner, “hydrophobic” core of the aggregates.

3.2. Interaction between CTEAB and DNA

Cationic surfactants have been considered for a few decades as potential non-viral vectors for gene delivery, thanks to their ability to easily form complexes with DNA. This complexation induces the formation of highly organized assemblies, involving various intermolecular interactions (electrostatic, hydrophobic, etc.) and highly cooperative binding.[39,40] In this field, CTAB was one of the most studied cationic surfactants. It has been shown that combination of electrostatic and hydrophobic interactions between CTAB and DNA induces functional and morphological changes of the biopolymer, particularly DNA compaction.[41–53] Considering CTEAB as a potential non-viral vector, it is therefore important to characterize the interactions occurring between the surfactant and the nucleic acid involved in such DNA formulations. It is especially interesting to study the effect of replacing CTAB by CTEAB on the different phase transitions, as we have shown that these structurally close surfactants differ, however, in their micellization properties.

Three macroscopic states were observed on CTEAB-DNA solutions depending on the CTEAB concentration. For [CTEAB] < 20-30×10^{-5} mol·L^{-1} clear solutions were observed. Between 20-30×10^{-5} mol.L^{-1} and 100-200 ×10^{-5} mol.L^{-1}, turbid solutions appear. For higher CTEAB concentrations ([CTEAB] > 100-200 ×10^{-5} mol.L^{-1}), turbid solutions turned to clear.

Therefore, complementary techniques (agarose gel electrophoresis, tensiometry, fluorimetry, UV-Visible spectrometry and circular dichroism) were used to study the binary system made of CTEAB and the supercoiled plasmid DNA pBR322 at various molar ratios.

Agarose gel electrophoresis was first carried out to study CTEAB-DNA interactions with CTEAB concentrations ranging from 0 to 4×10^{-3} mol·L^{-1} (Figure 5).

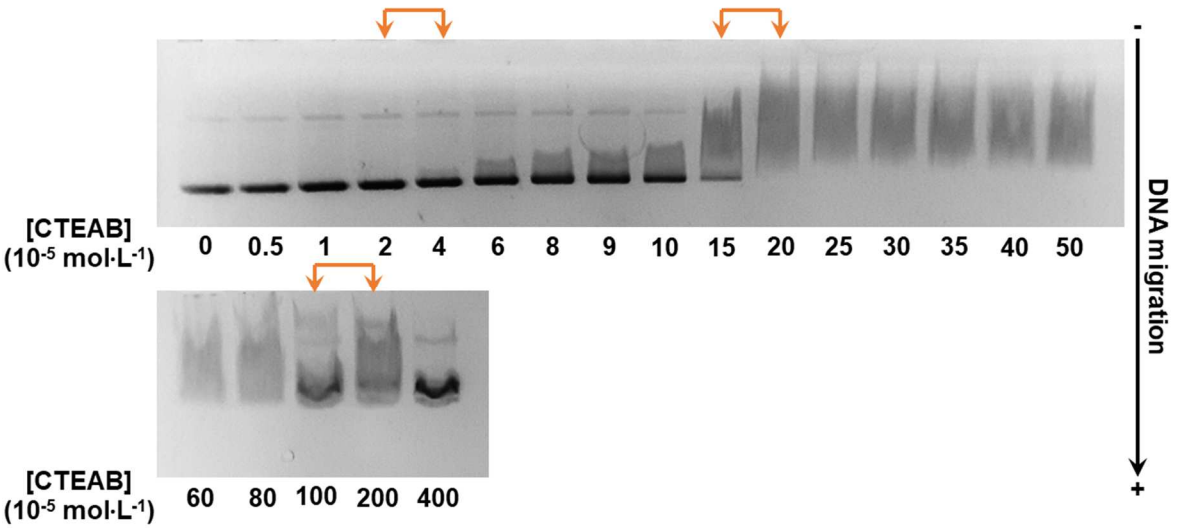

Figure 5. Electrophoresis agarose gel of plasmid DNA in the presence of various CTEAB concentrations (DNA concentration was [DNA-PO_4^-] = 9×10^{-5} mol·L^{-1}). Orange arrows indicate phase transitions.

Analysis of the electrophoresis agarose gel indicates the existence of different CTEAB-DNA interactions. At low CTEAB concentration, below 4×10^{-5} mol·L^{-1} ([CTEAB]/[DNA] = 0.44), the cooperative binding between DNA and CTEAB only slightly impacts the DNA mobility. In the second region, for 2-4×10^{-5} mol·L^{-1} < [CTEAB] < 15-20×10^{-5} mol·L^{-1}, (0.44 < [CTEAB]/[DNA] < 2.2) the complexation of CTEAB to DNA reduces the electrophoresis mobility of the DNA and a smear appears on the gel.[13] This results from the formation of aggregates between DNA and CTEAB, leading to the gradual compaction of DNA. Above 15-20×10^{-5} mol·L^{-1} ([CTEAB]/[DNA] = 2.2), the CTEAB-DNA compaction seems complete as it is no longer possible to observe the initial DNA band on the agarose gel. The

corresponding solutions appear slightly turbid. For CTEAB concentrations above 100×10^{-5} mol·L^{-1} ([CTEAB]/[DNA] = 11), the electrophoretic mobility of DNA seems to increase, with the re-apparition of a not-so-well defined band. This could indicate the formation of another type of CTEAB-DNA complex in the presence of a large excess of CTEAB and notably a decompaction process of DNA. In the litterature, this process was ascribed to the presence of an excess of the cationic surfactant, which promotes the DNA decompaction.[47,54,55] To go futher into the understanding of the interaction mechanisms between DNA and CTEAB, circular dichroism spectroscopy (CD) was realized. The DNA circular dichroic spectrum exhibits two peaks. The first one is a negative band at 245 nm, due to the helicity of DNA. The second one, at 278 nm is a positive band corresponding to the base stacking, as shown in Figure 6.[56–59]

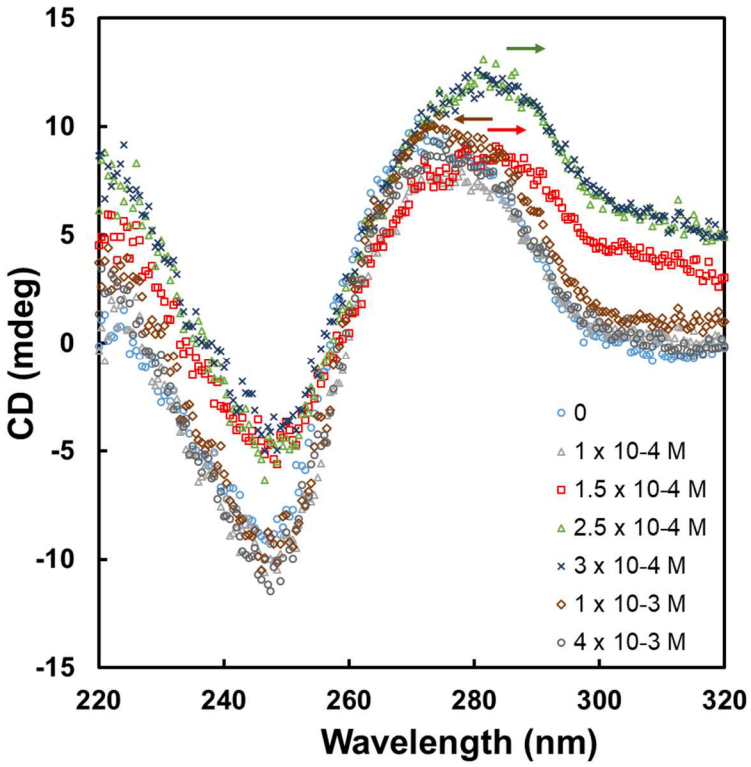

Figure 6. Circular dichroism spectra in CTEAB-DNA solutions for various CTEAB concentrations ([DNA-PO_4^-] = 9×10^{-5} mol·L^{-1}, 20 mM TRIS/HCl buffer, pH = 7.4) at 25 °C.

The CTEAB-DNA complexes, in the two phase regions, present a red-shift of the positive signal from 278 nm to 284 nm, for [CTEAB] > 15×10^{-5} mol.L^{-1}. This suggests a minor changing of interactions between the DNA bases and the evidence of the DNA compaction process in presence of CTEAB surfactant.[58] The observed transition could be due by the reduction of the DNA hydration layer, caused by a helical enhancement and a pitch shortening.[58,59] With further CTEAB concentration increase (from 100×10^{-5} mol.L^{-1}), there is a blue shift of the positive band and the position and intensity of that band recovers as DNA bands. It shows that CTEAB can decompact DNA with excessive amount of surfactant as it was already described in the literature for other surfactants.[47,54,55] These two peculiar CTEAB concentrations are on the same range that the ones find with the electrophoresis experiment.

CTEAB-DNA interactions were also evidenced by surface tension measurements. Figure 7A shows the variation of the surface tension of the DNA solution as a function of the CTEAB concentration.

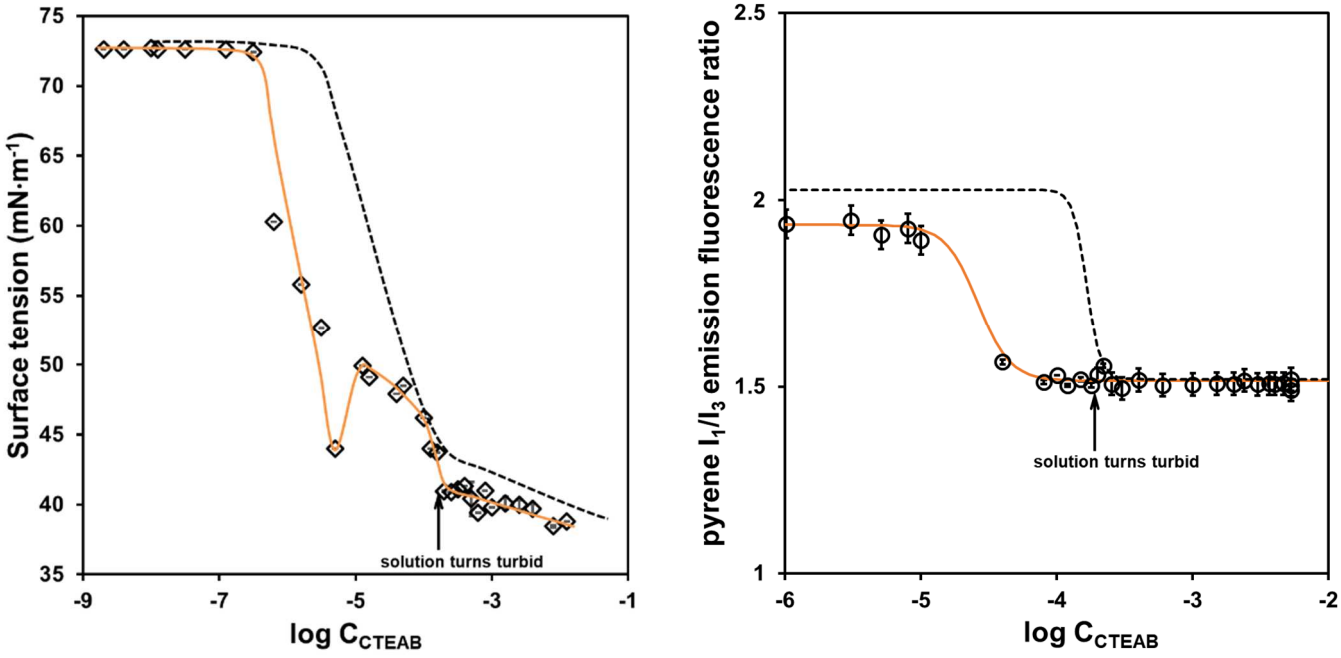

Figure 7. Variation of the surface tension (A), and of the pyrene I_1/I_3 fluorescence emission ratio (B) of CTEAB solutions as a function of CTEAB concentration, in the presence of DNA ([DNA-PO_4^-] = 9×10^{-5} mol·L^{-1}, 20 mM TRIS/HCl buffer, pH = 7.4) at 25 °C. Dashed lines refer to CTEAB alone, for comparison.

The curve profile obtained in the presence of DNA is more complex than the one for surfactant alone. Indeed, surface tension started to decrease at very low CTEAB concentrations (< 10^{-6} mol·L^{-1}) to reach a first minimum at [CTEAB] = 0.16×10^{-5} mol·L^{-1} ([CTEAB]/[DNA] = 0.02). It occurs well below the CMC of CTEAB, meaning that this phenomenon does not correspond to the formation of micelles. This rather shows the synergistic interaction between oppositely charged species that leads to the formation of highly surface active CTEAB-DNA complexes located at the air/water interface, as proposed by others.[41,60–62] This complexation is driven both by electrostatic interactions but also by hydrophobic interactions between the surfactant and the biopolymer.[41] In this concentration range, the CTEAB molecules are believed to gradually decorate the DNA strand by progressive charge neutralization. Then, upon increasing CTEAB concentration, the surface tension rises to a local maximum and finally decreases again and reaches the curve of pure CTEAB. This could be attributed to a partial desorption of the CTEAB-DNA complexes from the interface as they accumulate in the bulk solution upon adsorption of further surfactant, potentially forming new types of aggregates. Finally, the transition to a “plateau” coincides with the apparition of a turbid solution and is observed at [CTEAB] = 20×10^{-5} mol·L^{-1} ([CTEAB]/[DNA] = 2.2). At this point the polyanion is saturated with surfactant and the complex formed corresponds to formulated DNA. As the air/water interface is now

474 only occupied by surfactants, surface tension monitors then only the micellization of
475 CTEAB upon further addition of surfactant.

476 In a complementary way, pyrene fluorescence was studied at different
477 [CTEAB]/[DNA] ratios as previously conducted for CTEAB alone. In Figure 7B is
478 presented the variation of the pyrene I_1/I_3 emission fluorescence ratio as a function of
479 the CTEAB concentration in a DNA solution. We observed a classical sigmoidal
480 shape referring to a phase transition and the formation of hydrophobic domains.
481 Below the phase transition, the I_1/I_3 ratio was found to be 1.93 versus 2.03 in the
482 case of pure CTEAB. This slight decrease means that, even if pyrene is largely in
483 contact with water or in polar environment, it has found some more hydrophobic
484 places to locate. Indeed, it is known that pyrene can interact with DNA *via* partial
485 intercalation at the grooves.[63,64] Then the phase transition occurred at [CTEAB] =
486 2.8×10^{-5} mol·L^{-1} ([CTEAB]/[DNA] = 0.31). This critical concentration is much lower
487 than the CMC of pure CTEAB and refers here to a critical aggregation concentration
488 (CAC) evidencing again the synergistic aggregation of CTEAB and DNA. This point is
489 believed to refer to the transition between a state where DNA is decorated by
490 individual surfactant molecules (neutralization phase) and a state where CTEAB
491 molecules form local hydrophobic domains on the DNA strand (compaction phase).
492 Pyrene can locate in these aggregates and the I_1/I_3 ratio drops to the 1.51 value,
493 which is almost identical to what observed with CTEAB alone (1.50). This means that
494 pyrene still remains in a quite hydrated environment like in the case of CTEAB
495 micelles, where bulky head groups allow penetration of water. Note that the limited
496 decrease of the pyrene I_1/I_3 ratio does not allow the detection of further transitions as
497 observed for other DNA-cationic surfactant systems.[65,66] The steric hindrance of the
498 triethylammonium moiety could also explain why the transition occurs at a

[CTEAB]/[DNA] ratio which is much lower than in the case of CTAB (0.31 *vs.* about 0.70)[48]. Indeed, the neutralization phase is limited by the available space along the DNA strand and depends on the size of the complexing cationic surfactant.

The effect of the surfactant on DNA compaction can also be followed by UV-Vis spectrometry. Thus, DNA adsorption is performed at 260 nm for different CTEAB concentrations (Figure 8). It can be observed that absorption of CTEAB-DNA complex sharply decreases until a CTEAB concentration corresponding to 20-30×10^{-5} mol·L^{-1}. The increase in turbidity is due to strong electrostatic interactions between the DNA and the surfactant. This result suggests that DNA is fully compacted. CTEAB surfactant induces the reduction of the repulsive forces between the phosphate groups of DNA leading to the formation of CTEAB-DNA agregates.[56,57]

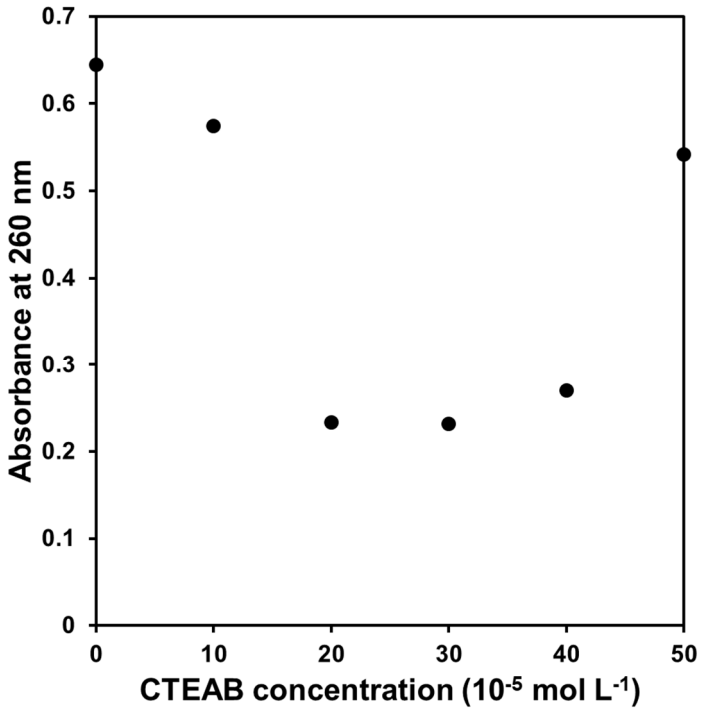

Figure 8. Variation of the absorbance of CTEAB-DNA solutions for various CTEAB concentrations at 260 nm ([DNA-PO_4^-] = 9×10^{-5} mol·L^{-1}, 20 mM TRIS/HCl buffer, pH = 7.4) at 25 °C

As the CTEAB concentration increases above 40×10^{-5} mol·L^{-1}, the absorbance value tends to recover to the origin value, ascribed to the decompaction process of DNA. The combination of these five complementary techniques has allowed to evidence different phase transitions for the CTEAB-DNA system depending on the surfactant concentration. They are summarized in Figure 9.

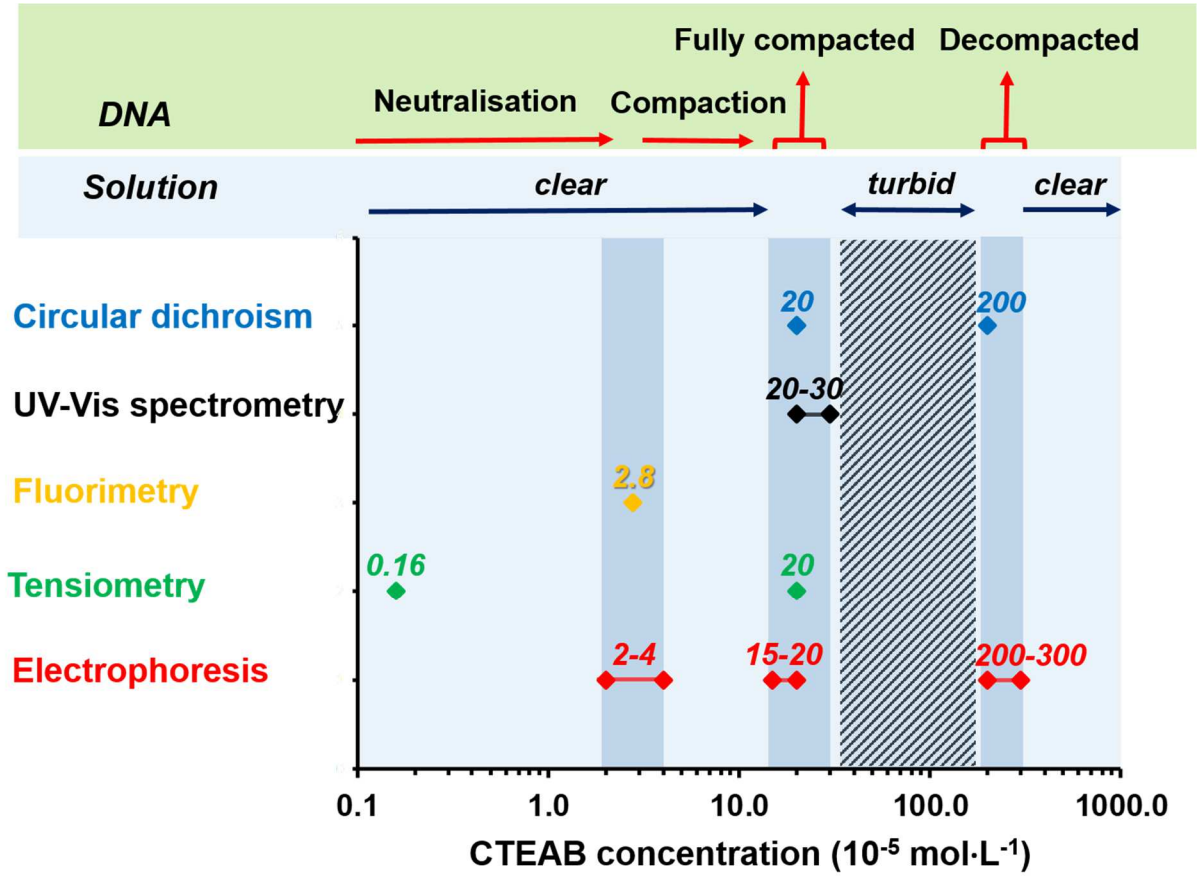

Figure 9. CTEAB concentrations (10^{-5} mol·L^{-1}) at which different phase transitions were evidenced by five complementary techniques in the CTEAB-DNA system (DNA concentration was [DNA-PO_4^-] = 9×10^{-5} mol·L^{-1} in 20 mM TRIS/HCl, pH = 7.4) at 25 °C.

The first transition occurring at very low concentration has been highlighted by surface tension measurements, and corresponds to the neutralization

529 ("lipophilization") of DNA by CTEAB. Next, agarose gel electrophoresis and
530 fluorimetry showed a phase transition towards a gradual compaction of DNA by
531 CTEAB. The end of this process, leading to a fully compacted DNA was evidenced
532 both by circular dichroism, UV-Vis spectroscopy, agarose gel electrophoresis and
533 surface tension measurements, as well as by macroscopic observations (solutions
534 became turbid). Finally, DNA decompaction was observed macroscopically and
535 highlighted by circular dichroism and agarose gel electrophoresis (DNA
536 redissolution).
537 The formulation of DNA was then studied under UVA radiation, in order to evaluate
538 the influence of compaction on DNA photodamage formation.

539 **3.3. Photostability of formulated DNA under UVA radiation**

540 Supercoiled pBR322 plasmid DNA was used as a DNA model to study the effect
541 of CTEAB surfactant on DNA damage under UVA radiation ($\lambda \geq 335$ nm).
542 Photolesions such as single-strand breaks (SSB) damage can be easily revealed by
543 agarose gel electrophoresis. Indeed, conversion of pBR322 plasmid DNA from the
544 supercoiled form (or Form I) to the circular form (or Form II) gives two distinctive
545 bands that can be separated and visualized by agarose gel electrophoresis (further
546 noted as **I** and **II** on the gel pictures, respectively), and quantified by
547 photodensitometry.

548 A first study was performed to show the effect of the irradiation time on the DNA
549 damage in the presence of CTEAB. On figure 10A, electrophoresis agarose gel
550 shows the DNA damage for irradiation times varying from 30 seconds to 10 minutes.
551 A progressive increase of single strand breaks (SSB) was observed with the increase
552 of the irradiation time. The quantification of the SSB ratios by photodensitometry
553 (Figure 10B) shows a linear increase of the SSB ratio for the shortest irradiation

554 times and its slow-down after 200 seconds to reach a SSB ratio of about 0.25 for 10
555 min irradiation.

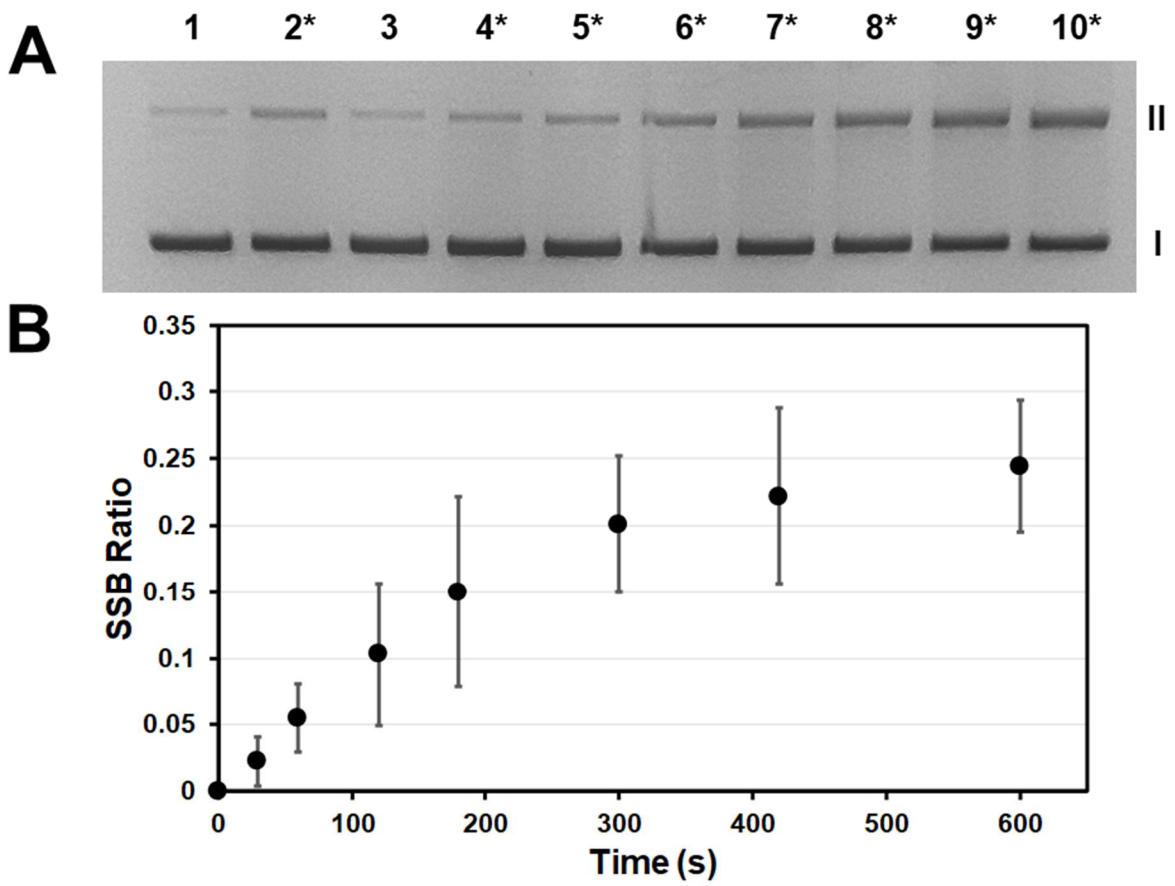

556

557 ***Figure 10. DNA cleavage for different irradiation times at λ ≥ 335nm and 20 °C (*
558 indicate the irradiated samples). A: Electrophoresis agarose gel of plasmid
559 pBR322 (9×10^{-5} mol·L^{-1}) with or without CTEAB (5×10^{-4} mol·L^{-1}) in 20 mM
560 TRIS/HCl buffer (pH = 7.4). Lane 1: DNA, t = 0 s; lane 2*: DNA, t = 10 min; lanes
561 3* to 10*: DNA with CTEAB, t = 0 s, 30 s, 1 min, 2 min, 3 min, 5 min, 7 min, and
562 10 min. B: Single strand break (SSB) ratio for different irradiation times as
563 quantified by photodensitometry.***

564

565 No longer time of irradiation was used because of the appearance of secondary DNA
566 strand breaks and the formation of pBR322 plasmid DNA linear form (data not show).

Control UVA irradiation of DNA alone also shows SSB damage that increase with irradiation time, but twice less than in the lipoplex (see agarose gel and photodensitometry quantification in the *Supporting Information*). DNA damage by UVA light were already described in the literature and different hypothesis were made to explain how DNA can be cleaved by UVA radiation whereas the nucleotides do not absorb at these wavelengths.[11,67–69] It has been shown that DNA solution presents a slight and broad absorbance band in UVA range which could be enough to induce UVA deterioration of DNA.[11,67] Recently, Markovitsi implied the existence of "collective" excited states in UVA photon absorption by DNA and speculated that condensed DNA enhanced the collective character of electronic excitations.[69] The CTEAB lipoplex made with the plasmid DNA pBR322 raises significantly the SSB ratio. The effect of the compaction of DNA induced by CTEAB could explain the increase of the DNA cleavage in the presence of surfactant. Indeed, Merindol *and al.* have shown the appearance of an absorption band on UVA wavelengths when DNA was aggregated by temperature.[70] To confirm this hypothesis, UV spectrum of the CTEAB-DNA complex was performed (see *Supporting Information*): a UVA absorption band appears in the presence of CTEAB. However, as the solution is turbid, the light scattering produced by the colloidal dispersion of the lipoplexes contributes to the UV-Vis spectrum and does not allow to differentiate the absorbance of the lipoplex from the scattering and to quantify each contribution.

The effect of the CTEAB concentration on the DNA photodamage was also studied and the irradiation time was fixed to 10 min. Indeed, this time allows to see well the formation of SSB while avoiding overbreaks. The CTEAB concentration range was from 0 to 7×10^{-4} mol·L^{-1} and corresponds to the lanes 2* to 9* on the

electrophoresis agarose gel shown in figure 11A. In figure 11B, the enhancement of the SSB ratio is shown with the increase of the CTEAB concentration.

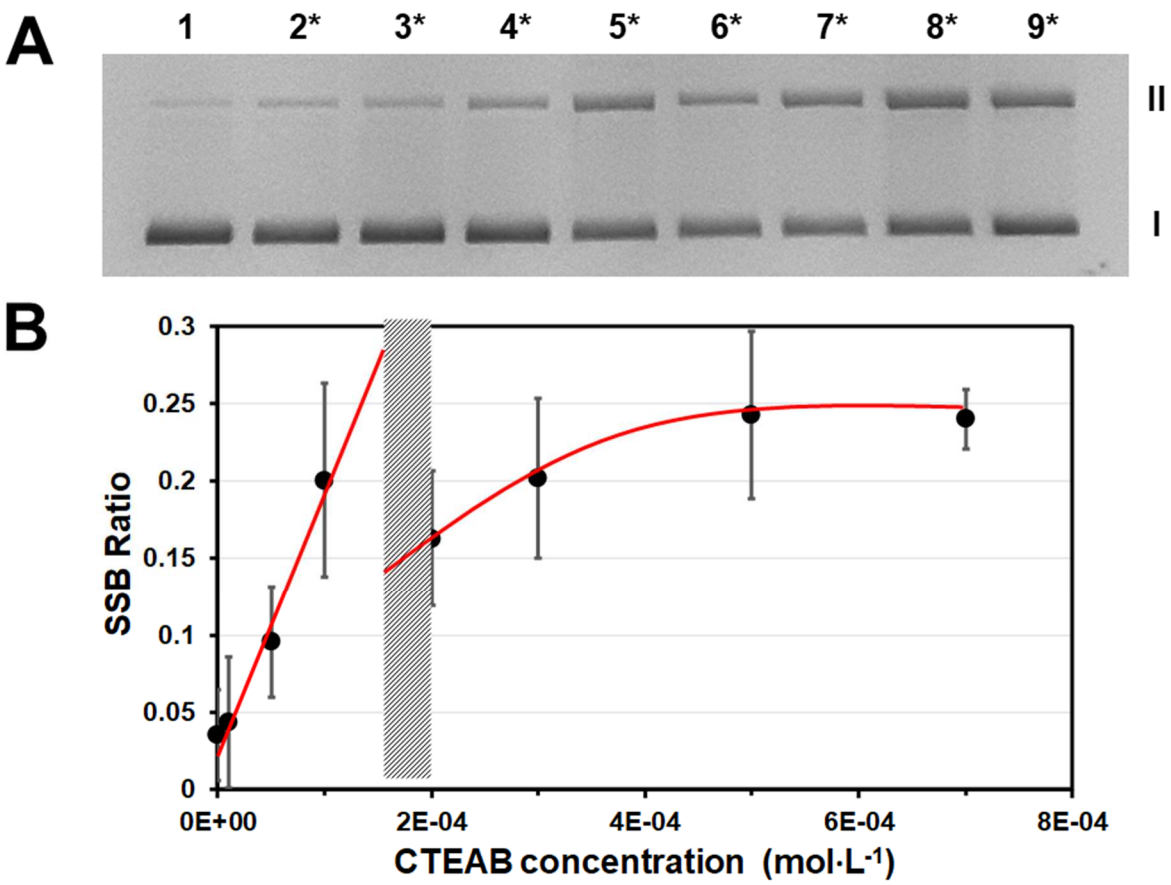

Figure 11. DNA cleavage for different CTEAB concentrations for 10 min irradiation at λ ≥ 335 nm and 20°C (* indicates the irradiated samples). A: Electrophoresis agarose gel of plasmid pBR322 (9×10^{-5} mol·L^{-1}) in 20 mM TRIS/HCl buffer (pH = 7.4). Lane 1: DNA alone without irradiation; lanes 2* to 10*: DNA with CTEAB irradiated, [CTEAB] = 0, 1×10^{-5}; 5×10^{-5}; 1×10^{-4}; 2×10^{-4}; 3×10^{-4}; 5×10^{-4}; 7×10^{-4} mol·L^{1}. B: Single strand break (SSB) ratio for different CTEAB concentrations.

Two distinct behaviors may be highlighted. For [CTEAB] ≤ 1×10^{-4} mol·L^{-1}, single-strand breaks increase linearly with CTEAB concentration. Higher concentrations

give rise to a second comportment which is not linear. The switch between these two regimes occurs at the characteristic phase transition shown above and corresponding to the full compaction of DNA by CTEAB.

Complementary experiments were undertaken to investigate the mechanism involved on the DNA damage formed during UVA irradiation of the CTEAB-DNA lipoplex.

One well-known damage induces by UVA irradiation of DNA is the formation of cyclobutane pyrimidine dimer (CPD)[11,71] and T4 endonuclease V is commonly used to detect CPD in UV irradiated DNA. Indeed, the presence of CPD on the supercoiled circular double-strand DNA induced a selective single-strand DNA scission by the DNA repair enzyme. The plasmid circular form (Form II) appears and can be revealed by agarose gel electrophoresis and quantified by photodensitometry as shown in Figure 12. DNA alone was treated with the phage T4 endonuclease V enzyme before and after 10 min of irradiation at $\lambda \geq 335$ nm (lanes 2 and 9*, Figure 12A). The enzymatic treatment reveals, by the AP-lyase activity of the T4 endonuclease V, the presence of abasic lesion on native plasmid DNA without irradiation (lane 2). When the DNA is irradiated and treated with T4 endonuclease (lane 9*), a significantly increase of the single-strand breaks is obtained. This is not due to the formation of the CPD mediated by UVA radiation, but to the photooxidized ones. Indeed, the SSB ratio with enzymatic treatment corresponds to the addition of the native damage in DNA (lane 2) and the photooxidized damage of irradiated DNA alone (lane 8*).

For the CTEAB-DNA lipoplex sample without irradiation and after T4 treatment (lane 7), the SSB ratio obtained is lower than DNA alone in the same condition (lane 2). The abasic lesions present in native DNA seem to be no revealed by the T4 enzyme

in presence of CTEAB surfactant. It could be due to the quenching of the T4 enzyme activity by CTEAB itself or that the enzyme doesn't have access to the lesions present on the non-irradiated compacted CTEAB-DNA lipoplex. But when the CTEAB-DNA lipoplex is irradiated and treated with the T4 endonuclease (lane 14*), single strand breaks are obtained. As for DNA alone, the observed damage enhancement corresponds to the accumulation of the photooxidized damage due to the CTEAB-DNA irradiation (lane 10*) and the abasic native DNA lesions (lane 2). On the irradiated sample, the T4 enzyme seems to have access again to the DNA damage. Our hypothesis is that the enzyme doesn't have access to the DNA because of its compaction in the non-irradiated CTEAB-DNA complex and that the photodegradation of the CTEAB-DNA complex induces a partial decompaction, enough to give back DNA accessible to the T4 enzyme.

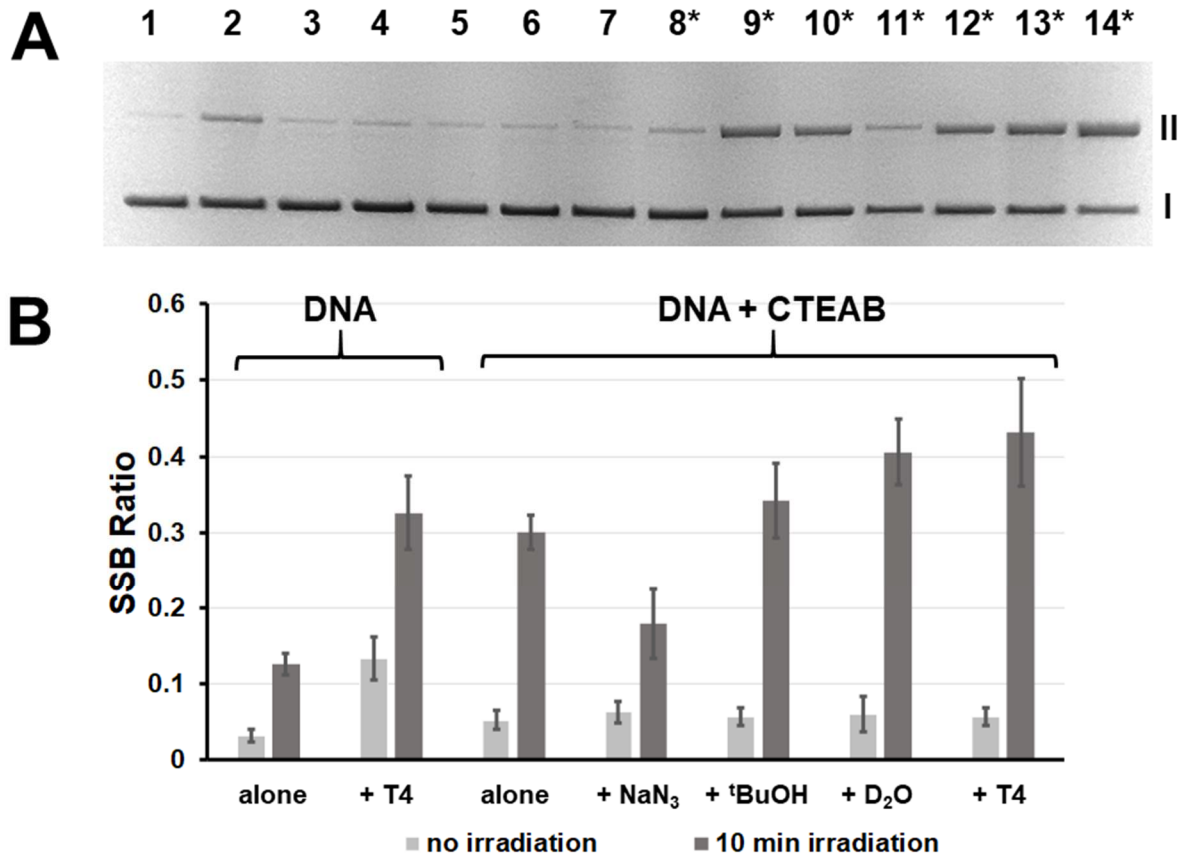

Figure 12. DNA cleavage for 10 min of irradiation at λ ≥ 335nm and 20°C with CTEAB (5×10^{-4} mol·L^{-1}) and NaN_3 (200×10^{-3} mol·L^{-1}), ^tBuOH (4% v/v), in D_2O (80% v/v) or phage T4 endonuclease V treatment (T4) (* indicates the irradiated samples). A: Electrophoresis agarose gel of plasmid pBR322 (9×10^{-5} mol·L^{-1}) in 20 mM TRIS/HCl buffer (pH = 7.4). Lanes 1 and 8*: DNA alone; lanes 2 and 9*: DNA + T4; lanes 3 and 10*: DNA + CTEAB; lanes 4 and 11*: DNA +CTEAB + NaN_3; lanes 5 and 12*: DNA +CTEAB + ^tBuOH; lanes 6 and 13*: DNA +CTEAB in D_2O; lanes 7 and 14*: DNA +CTEAB + T4. B: Single strand break (SSB) ratio of CTEAB-DNA lipoplex ± NaN_3, ^tBuOH, D_2O or T4 with and without irradiation.

To go further on the study of the mechanism involved in the formation of SSB, peculiar scavengers have been used. CTEAB-DNA lipoplex was first irradiated in presence of sodium azide NaN_3 (lane 11*), a well-known singlet oxygen quencher.[72] Under irradiation, the single-strand break ratio drops in presence of NaN_3 (Figure 12B). It means that the singlet oxygen is involved on the oxidized damage. To confirm it, the CTEAB-DNA lipoplex solution was also prepared in D_2O TRIS/DCl buffer and irradiated for 10 min (lane 13*). Indeed, D_2O increases the life time of the singlet oxygen,[73,74] and as expected an enhancement of SSB ratio is obtained (lane 13*). These results highlight the involvement of a type II mechanism by energy transfer from the DNA molecule itself, acting as a chromophore,[75] to the ground state of the molecular oxygen to produce the singlet oxygen responsible of these direct oxidized photodamage under UVA radiation. Finally, the lipoplex irradiation was performed with 4 % of tert-butanol (^tBuOH, lane 12*), as a OH radical scavenger.[76,77] No decrease of the SSB ratio is observable in the presence of ^tBuOH suggesting the

667 non-intervention of the type I mechanism involving hydroxyl radicals in these
668 processes.
669 In conclusion, UVA irradiation of DNA-CTEAB lipoplex induces the direct formation of
670 oxidized damage involving singlet oxygen and implementing energy transfer.
671 However, it does not lead to the formation of CPD. The compaction of the plasmid
672 pBR322 by the positive CTEAB surfactant is probably the cause of the increase in
673 photooxidized DNA damage.
674

675

4. Conclusion

677 Cationic surfactants or polymers have been shown to be efficient complexing agents
678 and transporters of DNA to cells. In this study, CTEAB surfactant was used to
679 complex a DNA model, the plasmid pBR322. The self-organization properties of the
680 CTEAB were studied by different physico-chemical characterizations (tensiometry,
681 pyrene fluorimetry and scattering experiments). Results show that CTEAB molecules
682 form small spherical and highly hydrated micelles in TRIS/HCl buffer solution. The
683 study of the interactions between CTEAB and plasmid DNA has highlighted different
684 phases, the DNA neutralization, the gradual until the full DNA compaction and the
685 decompaction process of DNA. Furthermore, formulated CTEAB-DNA lipoplexes
686 were irradiated under UVA light. With the increase of the irradiation time and of the
687 CTEAB concentration, an increase of DNA damage was observed. The involvement
688 of singlet oxygen has been shown to be responsible for these damage. The
689 compaction of DNA by CTEAB may be the cause of the increase in photooxidized
690 DNA damage. This study has investigated the DNA compaction by the cationic
691 surfactant CTEAB and pointed out its role on DNA photodamage under UVA
692 irradiation. Further work is currently under progress to show what could be the effect
693 of adding anti-oxidant drug such as vitamin E on the photodamage observed in this
694 system.

695

Acknowledgements

This work benefited from the use of the SasView application, originally developed under NSF award DMR-0520547. SasView contains code developed with funding from the European Union's Horizon 2020 research and innovation program under the SINE2020 project, grant agreement No 654000. Dr. C. Mingotaud is thanked for help in MULTI-STORMS use and for SAXS measurements.

References

(1) Foldvari, M.; Chen, D. W.; Nafissi, N.; Calderon, D.; Narsineni, L.; Rafiee, A. Non-Viral Gene Therapy: Gains and Challenges of Non-Invasive Administration Methods. *J. Control. Release* **2016**, *240*, 165–190. https://doi.org/10.1016/j.jconrel.2015.12.012.

(2) Dunbar, C. E.; High, K. A.; Joung, J. K.; Kohn, D. B.; Ozawa, K.; Sadelain, M. Gene Therapy Comes of Age. *Science (80-.).* **2018**, *359*, eaan4672. https://doi.org/10.1126/science.aan4672.

(3) Schuch, A. P.; Moreno, N. C.; Schuch, N. J.; Menck, C. F. M.; Garcia, C. C. M. Sunlight Damage to Cellular DNA: Focus on Oxidatively Generated Lesions. *Free Radic. Biol. Med.* **2017**, *107*, 110–124. https://doi.org/10.1016/j.electacta.2018.01.181.

(4) Tyrrell, R. M. Induction of Pyrimidine Dimers in Bacterial DNA by 365 Nm Radiation. *Photochem. Photobiol.* **1973**, *17*, 69–73. https://doi.org/10.1111/j.1751-1097.1973.tb06334.x.

(5) Kuluncsics, Z.; Perdiz, D.; Brulay, E.; Muel, B.; Sage, E. Wavelength Dependence of Ultraviolet-Induced DNA Damage Distribution : Involvement of Direct or Indirect Mechanisms and Possible Artefacts. *J. Photochem. Photobiol. B Biol.* **1999**, *49*, 71–80.

(6) Perdiz, D.; Gróf, P.; Mezzina, M.; Nikaido, O.; Moustacchi, E.; Sage, E. Distribution and Repair of Bipyrimidine Photoproducts in Solar UV-Irradiated Mammalian Cells: Possible Role of Dewar Photoproducts in Solar Mutagenesis. *J. Biol. Chem.* **2000**, *275* (35), 26732–26742. https://doi.org/10.1074/jbc.M001450200.

(7) Douki, T.; Reynaud-Angelin, A.; Cadet, J.; Sage, E. Bipyrimidine Photoproducts

Rather than Oxidative Lesions Are the Main Type of DNA Damage Involved in the Genotoxic Effect of Solar UVA Radiation. *Biochemistry* **2003**, *42* (30), 9221–9226. https://doi.org/10.1021/bi034593c.

(8) Mouret, S.; Baudouin, C.; Charveron, M.; Favier, A.; Cadet, J.; Douki, T. Cyclobutane Pyrimidine Dimers Are Predominant DNA Lesions in Whole Human Skin Exposed to UVA Radiation. *Proc. Natl. Acad. Sci.* **2006**, *103* (37), 13765–13770. https://doi.org/10.1073/pnas.0604213103.

(9) Schuch, A. P.; da Silva Galhardo, R.; de Lima-Bessa, K. M.; Schuch, N. J.; Menck, C. F. M. Development of a DNA-Dosimeter System for Monitoring the Effects of Solar-Ultraviolet Radiation. *Photochem. Photobiol. Sci.* **2009**, *8*, 111–120. https://doi.org/10.1039/b810085c.

(10) Jiang, Y.; Rabbi, M.; Kim, M.; Ke, C.; Lee, W.; Clark, R. L.; Mieczkowski, P. A.; Marszalek, P. E. UVA Generates Pyrimidine Dimers in DNA Directly. *Biophys. J.* **2009**, *96* (3), 1151–1158. https://doi.org/10.1016/j.bpj.2008.10.030.

(11) Mouret, S.; Philippe, C.; Gracia-Chantegrel, J.; Banyasz, A.; Karpati, S.; Markovitsi, D.; Douki, T. UVA-Induced Cyclobutane Pyrimidine Dimers in DNA: A Direct Photochemical Mechanism? *Org. Biomol. Chem.* **2010**, *8* (7), 1706–1711. https://doi.org/10.1039/b924712b.

(12) Cortat, B.; Garcia, C. C. M.; Quinet, A.; Schuch, A. P.; De Lima-Bessa, K. M.; Menck, C. F. M. The Relative Roles of DNA Damage Induced by UVA Irradiation in Human Cells. *Photochem. Photobiol. Sci.* **2013**, *12* (8), 1483–1495. https://doi.org/10.1039/c3pp50023c.

(13) Rudiuk, S.; Franceschi-Messant, S.; Chouini-Lalanne, N.; Perez, E.; Rico-Lattes, I. Modulation of Photo-Oxidative DNA Damage by Cationic Surfactant Complexation. *Langmuir* **2008**, *24* (16), 8452–8457.

https://doi.org/10.1021/la800751k.

(14) Davey, T. W.; Ducker, W. A.; Hayman, A. R.; Simpson, J. Krafft Temperature Depression in Quaternary Ammonium Bromide Surfactants. *Langmuir* **1998**, *14* (12), 3210–3213. https://doi.org/10.1021/la9711894.

(15) Israelachvili, J. N.; Mitchell, D. J.; Ninham, B. W. Theory of Self-Assembly of Hydrocarbon Amphiphiles into Micelles and Bilayers. *J. Chem. Soc. Faraday Trans. 2 Mol. Chem. Phys.* **1976**, 1525–1568. https://doi.org/10.1039/F29767201525.

(16) Wasbrough, M. J.; Edler, K. J.; Hawley, A. M.; Holdaway, J. A.; Price, G. J. Control of Mesostructure in Self-Assembled Polymer/Surfactant Films by Rational Micelle Design. *Soft Matter* **2012**, *8* (12), 3357–3362. https://doi.org/10.1039/c2sm07086c.

(17) Jaber, R.; Wasbrough, M. J.; Holdaway, J. A.; Edler, K. J. Interactions between Quaternary Ammonium Surfactants and Polyethylenimine at High PH in Film Forming Systems. *J. Colloid Interface Sci.* **2015**, *449*, 286–296. https://doi.org/10.1016/j.jcis.2015.01.034.

(18) Anderson, M. W.; Egger, C. C.; Tiddy, G. J. T.; Casci, J. L.; Brakke, K. A. A New Minimal Surface and the Structure of Mesoporous Silicas. *Angew. Chemie - Int. Ed.* **2005**, *44* (21), 3243–3248. https://doi.org/10.1002/anie.200462295.

(19) Kruk, M.; Jaroniec, M.; Sakamoto, Y.; Terasaki, O.; Ryoo, R.; Ko, C. H. Determination of Pore Size and Pore Wall Structure of MCM-41 by Using Nitrogen Adsorption, Transmission Electron Microscopy, and X-Ray Diffraction. *J. Phys. Chem. B* **2000**, *104* (2), 292–301. https://doi.org/10.1021/jp992718a.

(20) Huo, Q.; Margolese, D. I.; Ciesla, U.; Feng, P.; Gier, T. E.; Sieger, P.; Leon, R.; Petroff, P. M.; Schüth, F.; Stucky, G. D. Generalized Synthesis of Periodic

Surfactant/Inorganic Composite Materials. *Nature* **1994**, *368*, 317–321. https://doi.org/10.1038/368317a0.

(21) Gou, S.; Yin, T.; Yan, L.; Guo, Q. Water-Soluble Complexes of Hydrophobically Modified Polymer and Surface Active Imidazolium-Based Ionic Liquids for Enhancing Oil Recovery. *Colloids Surfaces A Physicochem. Eng. Asp.* **2015**, *471*, 45–53. https://doi.org/10.1016/j.colsurfa.2015.02.022.

(22) Li, X.; Xue, Q.; Wu, T.; Jin, Y.; Ling, C.; Lu, S. Oil Detachment from Silica Surface Modified by Carboxy Groups in Aqueous Cetyltriethylammonium Bromide Solution. *Appl. Surf. Sci.* **2015**, *353*, 1103–1111. https://doi.org/10.1016/j.apsusc.2015.07.014.

(23) Rosen, M. J.; Kunjappu, J. . *Surfactants and Interfacial Phenomena, 3rd Edition.*; 2012. https://doi.org/10.1002/0471670561.

(24) Kim, M. J.; Ryoo, R. Synthesis and Pore Size Control of Cubic Mesoporous Silica SBA-1. *Chem. Mater.* **1999**, *11*, 487–491. https://doi.org/10.1021/cm980691m.

(25) Ciulla, T. A.; Van Camp, J. R.; Resenfeld, A.; Kochevar, I. Photosensitization of Single-Strand Breaks in PBR322 DNA by Rose Bengal. *Photochem.* **1989**, *49* (3), 293–298.

(26) Soldi, V.; Keiper, J.; Romsted, L. S.; Cuccovia, I. M.; Chaimovich, H. Arenediazonium Salts: New Probes of the Interfacial Compositions of Association Colloids. 6. Relationships between Interfacial Counterion and Water Concentrations and Surfactant Headgroup Size, Sphere-to-Rod Transitions, and Chemical Reactivity in Cationi. *Langmuir* **2000**, *16*, 59–71. https://doi.org/10.1021/la990336q.

(27) Bacaloglu, R.; Bunton, C. A.; Ortega, F. Micellar Enhancements of Rates of

SN2 Reactions of Halide Ions. The Effect of Headgroup Size. *J. Phys. Chem.* **1989**, *93* (4), 1497–1502. https://doi.org/10.1021/j100341a061.

(28) Buckingham, S. A.; Garvey, C. J.; Warr, G. G. Effect of Head-Group Size on Micellization and Phase Behavior in Quaternary Ammonium Surfactant Systems. *J. Phys. Chem.* **1993**, *97* (39), 10236–10244. https://doi.org/10.1021/j100141a054.

(29) Rodríguez, M. A.; Muñoz, M.; Graciani, M. del M.; Fernández Pachón, M. S.; Moyá, M. L. Effects of Head Group Size on Micellization of Cetyltrialkylammonium Bromide Surfactants in Water-Ethylene Glycol Mixtures. *Colloids Surfaces A Physicochem. Eng. Asp.* **2007**, *298* (3), 177–185. https://doi.org/10.1016/j.colsurfa.2006.10.062.

(30) Haq, Z. U.; Rehman, N.; Ali, F.; Khan, N. M.; Hidayat, U. Effect of Electrolyte (NaCl) and Temperature on the Mechanism of Cetyl Trimethylammonium Bromide Micelles. *Sains Malaysiana* **2017**, *46* (5), 733–741.

(31) Kalyanasundaram, K.; Thomas, J. K. Environmental Effects on Vibronic Band Intensities in Pyrene Monomer Fluorescence and Their Application in Studies of Micellar Systems. *J. Am. Chem. Soc.* **1977**, *99* (7), 2039–2044. https://doi.org/10.1021/ja00449a004.

(32) Aguiar, J.; Carpena, P.; Molina-Bolívar, J. A.; Carnero Ruiz, C. On the Determination of the Critical Micelle Concentration by the Pyrene 1:3 Ratio Method. *J. Colloid Interface Sci.* **2003**, *258* (1), 116–122. https://doi.org/10.1016/S0021-9797(02)00082-6.

(33) Dong, D. C.; Winnik, M. A. The Py Scale of Solvent Polarities. *Canadian Journal of Chemistry*. 1984, pp 2560–2565. https://doi.org/10.1139/v84-437.

(34) Lianos, P.; Lang, J.; Sturm, J.; Zana, R. Fluorescence-Probe Study of Oil-in-

827 Water Microemulsions. 3. Further Investigations Involving Other Surfactants
828 and Oil Mixtures. *J. Phys. Chem.* **1984**, *88* (4), 819–822.
829 https://doi.org/10.1021/j150648a040.
830 (35) Frisken, B. J. Revisiting the Method of Cumulants for the Analysis of Dynamic
831 Light-Scattering Data. *Appl. Opt.* **2001**, *40* (24), 4087–4091.
832 (36) Pedersen, J. S. Analysis of Small-Angle Scattering Data from Colloids and
833 Polymer Solutions: Modeling and Least-Squares Fitting. *Adv. Colloid Interface*
834 *Sci.* **1997**, *70* (1–3), 171–210. https://doi.org/10.1016/S0001-8686(97)00312-6.
835 (37) Pedersen, J. S. Modelling of Small-Angle Scattering Date from Colloids and
836 Polymer Systems. In *Neutrons, X-rays and Light: Scattering Methods Applied*
837 *to Soft Condensed Matter*; 2002.
838 (38) Müller, W.; Déjugnat, C.; Zemb, T.; Dufreîche, J.-F.; Diat, O. How Do Anions
839 Affect Self-Assembly and Solubility of Cetylpyridinium Surfactants in Water. *J.*
840 *Phys. Chem. B* **2013**, *117* (5), 1345–1356. https://doi.org/10.1021/jp3093622.
841 (39) Liu, K.; Zheng, L.; Ma, C.; Göstl, R.; Herrmann, A. DNA-Surfactant Complexes:
842 Self-Assembly Properties and Applications. *Chem. Soc. Rev.* **2017**, *46*, 5147–
843 5172. https://doi.org/10.1039/c7cs00165g.
844 (40) Dias, R. S.; Pais, A. A. C. C.; Miguel, M. G.; Lindman, B. DNA and Surfactants
845 in Bulk and at Interfaces. *Colloids Surfaces A Physicochem. Eng. Asp.* **2004**,
846 *250*, 115–131. https://doi.org/10.1016/j.colsurfa.2004.07.026.
847 (41) Di Profio, P.; Germani, R.; Goracci, L.; Grilli, R.; Savelli, G.; Tiecco, M.
848 Interaction between DNA and Cationic Amphiphiles: A Multi-Technique Study.
849 *Langmuir* **2010**, *26* (11), 7885–7892. https://doi.org/10.1021/la9047825.
850 (42) Grueso, E.; Cerrillos, C.; Hidalgo, J.; Lopez-Cornejo, P. Compaction and
851 Decompaction of DNA Induced by the Cationic Surfactant CTAB. *Langmuir*

852 **2012**, *28* (30), 10968–10979. https://doi.org/10.1021/la302373m.
853 (43) Zhou, S.; Liang, D.; Burger, C.; Yeh, F.; Chu, B. Nanostructures of Complexes
854 Formed by Calf Thymus DNA Interacting with Cationic Surfactants.
855 *Biomacromolecules* **2004**, *5*, 1256–1261. https://doi.org/10.1021/bm034524d.
856 (44) Dias, R. S.; Innerlohinger, J.; Glatter, O.; Miguel, M. G.; Lindman, B. Coil-
857 Globule Transition of DNA Molecules Induced by Cationic Surfactants: A
858 Dynamic Light Scattering Study. *J. Phys. Chem. B* **2005**, *109*, 10458–10463.
859 https://doi.org/10.1021/jp0444464.
860 (45) Zhu, D.; Evans, R. K.; August, R. V; Final, I.; January, F. Molecular Mechanism
861 and Thermodynamics Study of Plasmid DNA and Cationic Surfactants
862 Interactions. *Langmuir* **2006**, *22*, 3735–3743.
863 (46) Guo, Q.; Zhang, Z.; Song, Y.; Liu, S.; Gao, W.; Qiao, H.; Guo, L.; Wang, J.
864 Investigation on Interaction of DNA and Several Cationic Surfactants with
865 Different Head Groups by Spectroscopy, Gel Electrophoresis and Viscosity
866 Technologies. *Chemosphere* **2017**, *168*, 599–605.
867 https://doi.org/10.1016/j.chemosphere.2016.11.019.
868 (47) Li, X.; Sun, D.; Chen, Y.; Wang, K.; He, Q.; Wang, G. Studying Compaction-
869 Decompaction of DNA Molecules Induced by Surfactants. *Biochem. Biophys.*
870 *Res. Commun.* **2018**, *495* (4), 2559–2565.
871 https://doi.org/10.1016/j.bbrc.2017.12.151.
872 (48) Mel'nikov, S. M.; Sergeyev, V. G.; Yoshikawa, K. Transition of Double-
873 Stranded DNA Chains between Random Coil and Compact Globule States
874 Induced by Cooperative Binding of Cationic Surfactant. *J. Am. Chem. Soc.*
875 **1995**, *117*, 2401–2408.
876 (49) Mel'nikov, S. M.; Yoshikawa, K. Discrete Coil-Globule Transition of Large DNA

Induced by Cationic Surfactant. *J. Am. Chem. Soc.* **1995**, *117*, 2401–2408.

(50) Mel'nikov, S. M.; Sergeyev, V. G.; Yoshikawa, K.; Takahashi, H.; Hatta, I. Cooperativity or Phase Transition ? Unfolding Transition of DNA Cationic Surfactant Complex Cooperativity or Phase Transition ? Unfolding Transition of DNA Cationic Surfactant Complex. *J. Chem. Phys.* **1997**, *107* (17), 6917–6924. https://doi.org/10.1063/1.474932.

(51) Sergeyev, V. G.; Mikhailenko, S. V.; Pyshkina, O. A.; Yaminsky, I. V.; Yoshikawa, K. How Does Alcohol Dissolve the Complex of DNA with a Cationic Surfactant? *J. Am. Chem. Soc.* **1999**, *121*, 1780–1785. https://doi.org/10.1021/ja981683+.

(52) Clamme, J. P.; Bernacchi, S.; Vuilleumier, C.; Duportail, G.; Mély, Y. Gene Transfer by Cationic Surfactants Is Essentially Limited by the Trapping of the Surfactant/DNA Complexes onto the Cell Membrane: A Fluorescence Investigation. *Biochim. Biophys. Acta - Biomembr.* **2000**, *1467*, 347–361. https://doi.org/10.1016/S0005-2736(00)00230-3.

(53) Dias, R.; Mel, S.; Miguel, M. G. DNA Phase Behavior in the Presence of Oppositely Charged Surfactants. *Langmuir* **2000**, *16*, 9577–9583.

(54) Xu, L.; Feng, L.; Hao, J.; Dong, S. Compaction and Decompaction of DNA Dominated by the Competition between Counterions and DNA Associating with Cationic Aggregates. *Colloids Surfaces B Biointerfaces* **2015**, *134*, 105–112. https://doi.org/10.1016/j.colsurfb.2015.06.038.

(55) Feng, L.; Xu, L.; Hao, J.; Dong, S. Controlled Compaction and Decompaction of DNA by Zwitterionic Surfactants. *Colloids Surfaces A Physicochem. Eng. Asp.* **2016**, *501*, 65–74. https://doi.org/10.1016/j.colsurfa.2016.04.052.

(56) Wang, L.; Wang, Y.; Hao, J.; Dong, S. Magnetic Fullerene-DNA / Hyaluronic

902 Acid Nanovehicles with Magnetism / Reduction Dual-Responsive Triggered
903 Release. *Biomacromolecules* **2017**, *18*, 1029–1038.
904 https://doi.org/10.1021/acs.biomac.6b01939.
905 (57) Wang, L.; Wang, Y.; Dong, S.; Deng, Y.; Hao, J. Nanocapsules of Magnetic Au
906 Self-Assembly for DNA Migration and Secondary Self-Assembly. *ACS Appl.*
907 *Mater. Interfaces* **2018**, *10*, 5348–5357.
908 https://doi.org/10.1021/acsami.7b18689.
909 (58) Wang, L.; Wang, Y.; Sun, X.; Zhang, G.; Dong, S. Versatile Self-Assembly and
910 Biosensing Applications of DNA and Carbon Quantum Dots Coordinated
911 Cerium Ions. *ChemPubSocEurope* **2017**, *23*, 10413–10422.
912 https://doi.org/10.1002/chem.201701709.
913 (59) Wang, L.; Wang, G.; Wang, Y.; Liu, H.; Dong, S.; Hao, J. Fluorescent Hybrid
914 Nanospheres Induced by Single-Stranded DNA and Magnetic Carbon
915 Quantum Dots. *New J. Chem.* **2019**, *43*, 4965–4974.
916 https://doi.org/10.1039/c8nj06157b.
917 (60) McLoughlin, D.; Langevin, D. Surface Complexation of DNA with a Cationic
918 Surfactant. *Colloids Surfaces A Physicochem. Eng. Asp.* **2004**, *250*, 79–87.
919 https://doi.org/10.1016/j.colsurfa.2004.04.096.
920 (61) Moradi, N.; Zakrevskyy, Y.; Javadi, A.; Aksenenko, E. V.; Fainerman, V. B.;
921 Lomadze, N.; Santer, S.; Miller, R. Surface Tension and Dilation Rheology of
922 DNA Solutions in Mixtures with Azobenzene-Containing Cationic Surfactant.
923 *Colloids Surfaces A Physicochem. Eng. Asp.* **2016**, *505*, 186–192.
924 https://doi.org/10.1016/j.colsurfa.2016.04.021.
925 (62) Lyadinskaya, V. V.; Lin, S. Y.; Michailov, A. V.; Povolotskiy, A. V.; Noskov, B.
926 A. Phase Transitions in DNA/Surfactant Adsorption Layers. *Langmuir* **2016**, *32*,

13435–13445. https://doi.org/10.1021/acs.langmuir.6b03396.

(63) Jumbri, K.; Rahman, M. B. A.; Abdulmalek, E.; Ahmad, H.; Micaelo, N. M. An Insight into Structure and Stability of DNA in and Experimental Studies. *Phys. Chem. Chem. Phys.* **2014**, *16*, 14036–14046. https://doi.org/10.1039/c4cp01159g.

(64) Wang, H.; Wang, J.; Zhang, S. Binding Gibbs Energy of Ionic Liquids to Calf Thymus DNA: A Fluorescence Spectroscopy Study. *Phys. Chem. Chem. Phys.* **2011**, *13*, 3906–3910. https://doi.org/10.1039/c0cp01815e.

(65) Petrov, A. I.; Khalil, D. N.; Kazaryan, R. L.; Savintsev, I. V.; Sukhorukov, B. I. Structural and Thermodynamic Features of Complexes Formed by DNA and Synthetic Polynucleotides with Dodecylamine and Dodecyltrimethylammonium Bromide. *Bioelectrochemistry* **2002**, *58*, 75–85. https://doi.org/10.1016/S1567-5394(02)00130-5.

(66) Zhang, L.; Dong, Y.; Zhang, X.; Guo, X. Micellization of Lactosylammonium Surfactants with Di Ff Erent Counter Ions and Their Interaction with DNA. *J. Chem. Eng. Data* **2016**, *61*, 2969–2978. https://doi.org/10.1021/acs.jced.5b01057.

(67) Sutherland, J. C.; Griffin, K. P. Absorption Spectrum of DNA for Wavelengths Greater than 300 Nm. *Radiat. Res.* **1981**, *86* (3), 399–410.

(68) Ikehata, H. Mechanistic Considerations on the Wavelength- Dependent Variations of UVR Genotoxicity and Mutagenesis in Skin : The Discrimination of UVA- Signature from UV-Signature Mutation. *Photochem. Photobiol. Sci.* **2018**. https://doi.org/10.1039/c7pp00360a.

(69) Markovitsi, D. UV-Induced DNA Damage: The Role of Electronic Excited States. *Photochem. Photobiol.* **2016**, *92*, 45–51.

952 https://doi.org/10.1111/php.12533.
953 (70) Merindol, R.; Loescher, S.; Samanta, A.; Walther, A. Pathway-Controlled
954 Formation of Mesostructured All-DNA Colloids and Superstructures. *Nat.*
955 *Nanotechnol.* **2018**, *13*, 730–738. https://doi.org/10.1038/s41565-018-0168-1.
956 (71) Cadet, J.; Douki, T. Formation of UV-Induced DNA Damage Contributing to
957 Skin Cancer Development. *Photochem Photobiol. Sci.* **2018**, *17*, 1816–1841.
958 https://doi.org/10.1039/c7pp00395a.
959 (72) Bancirova, M. Sodium Azide as a Specific Quencher of Singlet Oxygen during
960 Chemiluminescent Detection by Luminol and Cypridina Luciferin Analogues.
961 *Luminescence* **2011**, *26* (6), 685–688. https://doi.org/10.1002/bio.1296.
962 (73) Merkel, P. B.; Nilsson, R.; Kearns, D. R. Deuterium Effects on Singlet Oxygen
963 Lifetimes in Solutions. New Test of Singlet Oxygen Reactions. *J. Am. Chem.*
964 *Soc.* **1972**, *94* (3), 1030–1031. https://doi.org/10.1021/ja00758a072.
965 (74) Merkel, P. B.; Kearns, D. R. Radiationless Decay of Singlet Molecular Oxygen
966 in Solution. Experimental and Theoretical Study of Electronic-to-Vibrational
967 Energy Transfer. *J. Am. Chem. Soc.* **1972**, *94* (21), 7244–7253.
968 https://doi.org/10.1021/ja00776a003.
969 (75) Yagura, T.; Passaglia, A.; Carrião, C.; Garcia, M.; Ribeiro, C.; Rocha, R.;
970 Cestari, N.; Pedro, J.; Angeli, F.; Mendes, D.; et al. Free Radical Biology and
971 Medicine Direct Participation of DNA in the Formation of Singlet Oxygen and
972 Base Damage under UVA Irradiation. *Free Radic. Biol. Med.* **2017**, *108*, 86–93.
973 https://doi.org/10.1016/j.freeradbiomed.2017.03.018.
974 (76) Billen, D. The Role of Hydroxyl Radical Scavengers in Preventing DNA Strand
975 Breaks Induced by X Irradiation of Toluene-Treated Escherichia Coli. *Radiat.*
976 *Res.* **1984**, *97* (3), 626–629.

(77) Staehelln, J.; Hoigné, J. Decomposition of Ozone in Water in the Presence of Organic Solutes Acting as Promoters and Inhibitors of Radical Chain Reactions. *Environ. Sci. Technol.* **1985**, *19* (12), 1206–1213. https://doi.org/10.1021/es00142a012.

Table of contents